Available online at www.sciencedirect.com
SCIENCE DIRECT®
Phytochemistry 66 (2005) 2632–2642
PHYTOCHEMISTRY
www.elsevier.com/locate/phytochem

Changes in flux pattern of the central carbohydrate metabolism during kernel development in maize

Christian Ettenhuber [a,1], Gertraud Spielbauer [b,1], Lilla Margl [b], L. Curtis Hannah [c], Alfons Gierl [b], Adelbert Bacher [a], Ulrich Genschel [b], Wolfgang Eisenreich [a,*]

[a] Lehrstuhl für Organische Chemie und Biochemie, Technische Universität München, Lichtenbergstr. 4, D-85747 Garching, Germany
[b] Lehrstuhl für Genetik, Technische Universität München, Am Hochanger 8, 85350 Freising, Germany
[c] Horticultural Sciences Department, University of Florida, Gainesville, FL 32611, United States

Received 20 May 2005; received in revised form 15 September 2005
Available online 7 November 2005

Abstract

Developing kernels of the inbred maize line W22 were grown in sterile culture and supplied with a mixture of [U–$^{13}C_6$]glucose and unlabeled glucose during three consecutive intervals (11–18, 18–25, or 25–32 days after pollination) within the linear phase of starch formation. At the end of each labeling period, glucose was prepared from starch and analyzed by ^{13}C isotope ratio mass spectrometry and high-resolution ^{13}C NMR spectroscopy. The abundances of individual glucose isotopologs were calculated by computational deconvolution of the NMR data. [1,2-$^{13}C_2$]-, [5,6-$^{13}C_2$]-, [2,3-$^{13}C_2$]-, [4,5-$^{13}C_2$]-, [1,2,3-$^{13}C_3$]-, [4,5,6-$^{13}C_3$]-, [3,4,5,6-$^{13}C_4$]-, and [U–$^{13}C_6$]-isotopologs were detected as the major multiple-labeled glucose species, albeit at different normalized abundances in the three intervals. Relative flux contributions by five different pathways in the primary carbohydrate metabolism were determined by computational simulation of the isotopolog space of glucose. The relative fractions of some of these processes in the overall glucose cycling changed significantly during maize kernel development. The simulation showed that cycling via the non-oxidative pentose phosphate pathway was lowest during the middle interval of the experiment. The observed flux pattern could by explained by a low demand for amino acid precursors recruited from the pentose phosphate pathway during the middle interval of kernel development.

Keywords: *Zea mays*; Kernel culture; NMR spectroscopy; Starch; Carbohydrate cycling; ^{13}C-glucose

1. Introduction

Grass seeds including wheat, maize, rice, barley and oats are the most important staple for human nutrition and have an important role in animal husbandry. Impressive increases of productivity have been obtained by classical breeding methods. Thus, the productivity of maize can be raised by approximately 1% per year (Duvick, 2001). Whereas plant genetics and biochemistry have been progressing rapidly in recent years, most noticeable with the sequencing of the genomes of *Arabidopsis thaliana* (Arabidopsis Genome Initiative, 2001; Yamada et al., 2003) and rice (Goff et al., 2002), transformation of this molecular information into enhanced yields of crop plants remains problematic.

It is generally agreed that the assessment of metabolite flux could broaden the basis for rational plant breeding. However, the reconstruction of flux parameters from genomic and proteomic data is faced with many uncertainties. Direct and sensitive methods are therefore required for the quantitative assessment of metabolite flux in plants.

Abbreviations: DAP, days after pollination; IRMS, isotope-ratio mass spectroscopy; NMR, nuclear magnetic resonance; PPP, pentose phosphate pathway.

* Corresponding author. Tel.: +49 89 289 13336; fax: +49 89 289 13363.
E-mail address: wolfgang.eisenreich@ch.tum.de (W. Eisenreich).

[1] These authors contributed equally to the work.

0031-9422/$ - see front matter © 2005 Elsevier Ltd. All rights reserved.
doi:10.1016/j.phytochem.2005.09.017

Stable isotopolog perturbation analysis can serve that purpose (Dieuaide-Noubhani et al., 1995; Glawischnig et al., 2001; Kruger et al., 2003; Eisenreich et al., 2004; Schwender et al., 2004; Sriram et al., 2004). The quasi-equilibrium state of isotope distribution can be perturbed by the introduction of isotope-labeled compounds into the system under study. Such a perturbation will subsequently spread through the entire metabolic network due to the catalytic activity of thousands of plant enzymes.

Pathways of the intermediary metabolism were identified and quantified in maize root tips growing in the presence of [1-^{13}C]glucose (Dieuaide-Noubhani et al., 1995; Edwards et al., 1998). The ^{13}C-enrichments of free glucose, sucrose, alanine, glutamate, and starch glucose were numerically fitted using a metabolic model including sucrose cycling, glycolysis, the transaldolase reaction of the pentose phosphate pathway (PPP), and the tricarboxylic acid cycle.

Analysis of glycolytic and PPP flux in developing embryos of *Brassica napus* (Schwender et al., 2003) revealed cycling between hexose phosphates and triose phosphates and the reversible transketolase reaction as the largest fluxes, while flux through the reversible transaldolase reaction was very low. More recently, an extended metabolic network model was applied to developing soybean embryos (Sriram et al., 2004), enabling the detection of compartmented parallel fluxes. Soybean embryos also showed intensive cycling between hexose phosphates and triose phosphates, but, in contrast to the situation in *Brassica*, there was a large flux through the oxidative part of the PPP and reversible transketolase and transaldolase fluxes were similar.

All these studies were based on the analysis of multiple metabolites (e.g., carbohydrates and amino acids). As shown in this paper, highly significant information about metabolite flux can also be obtained by the comprehensive analysis of a single metabolite, in this case glucose isolated from starch hydrolysate. The biosynthesis of starch in the storage tissue of monocotyledonous plants has been studied in considerable detail (for review, see Ball and Morell, 2003; Schultz and Juvik, 2004). In the endosperm, ADP-glucose is predominantly synthesized in the cytosol and transported into the amyloplast, where it is converted into starch by starch synthases, branching enzymes and debranching enzymes (James et al., 2003). However, while the topology of carbohydrate and starch metabolism is understood in some detail, quantification of in vivo fluxes within this metabolic network has been reported in few cases only.

Previously, we showed that [U–$^{13}C_6$]glucose is converted into a variety of ^{13}C-labeled isotopologs of starch glucose by developing maize kernels (Glawischnig et al., 2002). This experimental approach revealed the metabolic history of glucose, i.e., its extensive processing by the network of primary carbohydrate metabolism. Using an improved experimental setup and computational simulation, we now quantified the contribution of individual pathways to the metabolic cycling of glucose in maize kernels between 11 and 32 days after pollination (DAP). During the seemingly uniform process of starch deposition, both the metabolic flux pattern and the intensity of carbohydrate cycling showed appreciable changes.

2. Results

Kernels of the inbred maize line W22 were grown on tissue culture medium in the absence of ^{13}C label until 11 DAP, 18 DAP, or 25 DAP, respectively. Kernels were then transferred onto [U–$^{13}C_6$]glucose-containing medium for 7 days and subsequently harvested (cf. Fig. 1(a)). Starch was isolated from these kernels and hydrolyzed to glucose, which was used for analysis of ^{13}C-labeling patterns. Using the same tissue culture process, the accumulation of dry biomass was found to be approximately linear between 9 and 38 DAP (Fig. 1(b)).

In the ^{13}C-labeling medium, glucose with natural ^{13}C-abundance was present at 29-fold molar excess over [U–$^{13}C_6$]glucose. Total ^{13}C-enrichments of starch glucose from the 11–18 DAP, 18–25 DAP, and 25–32 DAP labeling experiments were determined by ^{13}C-isotope ratio mass spectrometry as 2.53%, 2.08%, and 1.87%, respectively. A successive decrease in the ^{13}C-enrichments is expected because the starch formed during the presence of [U–$^{13}C_6$]glucose is diluted by an increasing amount of preformed natural ^{13}C-abundance starch in the older kernels.

The isotopolog composition of glucose was determined from the quantitative analysis of high-resolution ^{13}C NMR spectra (Eisenreich et al., 2004). Due to ^{13}C^{13}C coupling, all ^{13}C signals of glucose appeared as complex

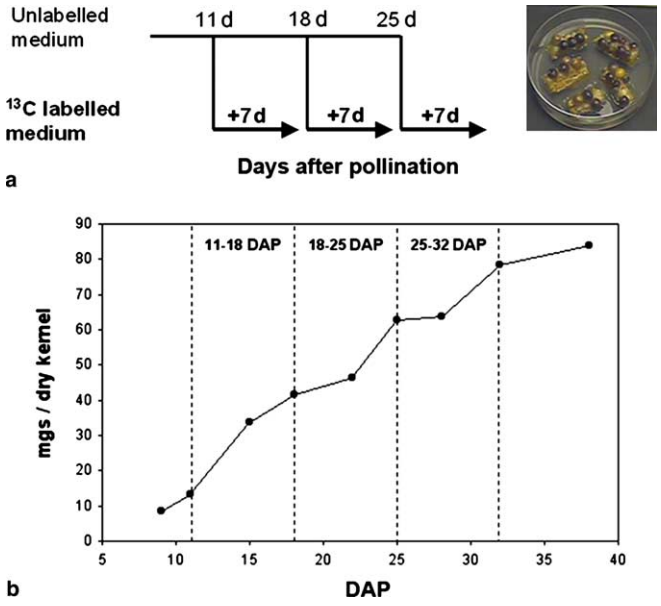

Fig. 1. (a) Experimental schedule for maize kernel culture and labeling scheme. At 11, 18, and 25 days after pollination, maize kernels were transferred onto labeled culture medium for 7 days and then harvested. (b) Increase of kernel dry weight in sterile culture from 9 to 38 DAP. The three intervals chosen for ^{13}C-labeling are indicated.

multiplets (Supplemental Tables 2 and 3). The situation was further complicated by the presence of two glucose anomers (α- and β-glucose, respectively) which are in a state of equilibrium in the aqueous solution of the NMR samples.

In order to simplify the description of complex isotopolog mixtures, we introduced a specialized notation for the isotopologs of glucose (Eisenreich et al., 2004). The carbon skeleton of glucose is represented by a six-digit binary number where the first digit represents C-1, the second digit represents C-2, etc.; 1 (one) signifies ^{13}C, 0 (zero) signifies ^{12}C, and X signifies either ^{12}C or ^{13}C. For example, {100000} designates [1-$^{13}C_1$]glucose, {000111} designates [4,5,6-$^{13}C_3$]glucose, and {110XXX} designates a set of isotopologs carrying ^{13}C in positions 1 and 2, ^{12}C in position in position 3, and ^{13}C or ^{12}C in any of the positions 4 through 6; sets of this type are subsequently designated as X groups.

Due to the fact that some of the long-range ^{13}C-coupling constants cannot be resolved in the ^{13}C NMR spectrum of glucose, individual spectral signatures fail to directly determine the abundances of individual isotopologs. However, the presence of certain sets of isotopologs (X groups) is correlated with specific signals on the basis of the known ^{13}C coupling constants and isotope shifts of glucose (Eisenreich et al., 2004). As an example, the ^{13}C NMR signals of C-1β, C-4α and C-4β of glucose from starch kernels in the present study can be assigned to {1XXXXX} and {XXX1XX} and their 10 subgroups shown in Fig. 2. It can be seen that the signal ratios between central peaks and corresponding

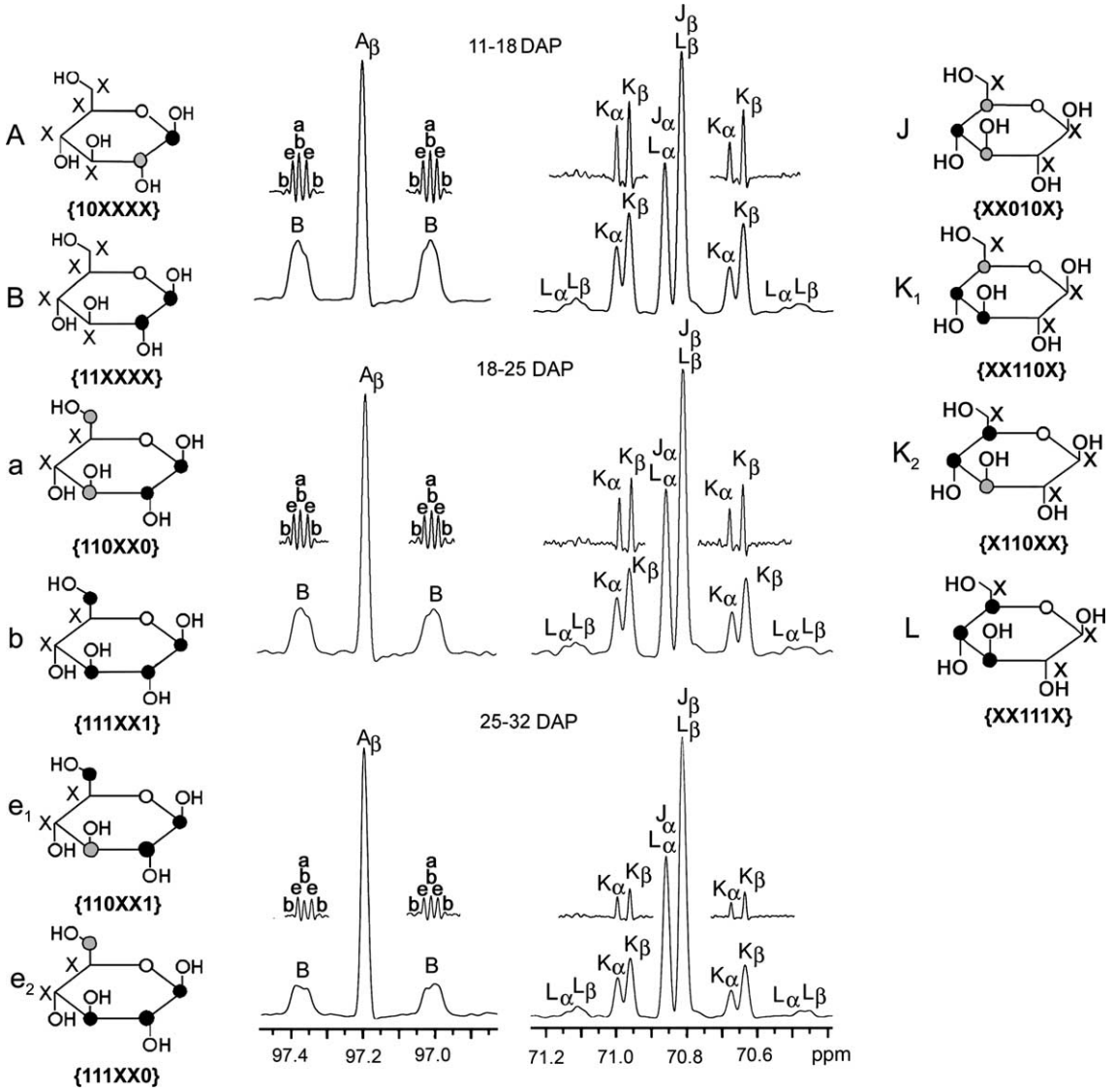

Fig. 2. ^{13}C NMR signals of glucose from starch hydrolysate with kernels 11–18, 18–25 and 25–32 days after pollination. Signals of C-1β (97.20 ppm), C-4α (70.90 ppm), and C-4β (70.83 ppm) are shown with their corresponding X groups (1 = ^{13}C, 0 = ^{12}C and X = ^{13}C or ^{12}C). Filled and shadowed circles in the structures indicate ^{13}C and ^{12}C, respectively. Undetermined positions (^{12}C or ^{13}C) are indicated by 'X'. Signal sections shown on top of a given signal group are calculated with a 'strong' Gaussian function (LB = −2, GB = 0.4). Signal intensities of corresponding atoms are normalized to the intensities of the central peaks.

satellite peaks (for example, A versus B or J versus L/K), as well as the signal ratios between distinct satellite peaks of different signal sets (for example, e versus a/b) are modulated over the experimental time period.

Earlier, we showed that the abundances of individual isotopologs can be determined from the X group abundance data by deconvolution using a genetic algorithm (Eisenreich et al., 2004; Ettenhuber et al., 2005). More specifically, the abundances of the X groups serve as constraints in the calculation of the abundances of individual isotopologs. The convergence behavior of this deconvolution process for glucose X groups from the three labeling intervals is shown in Fig. 3. The evolution process shows convergence in less than 3000 iterations. Evolutions in jumps and intervals of oscillation indicate that the sample from 11–18 DAP has a sharp minimum in a complex landscape of the isotopolog state space, whereas the minima for the sample from 18–25 DAP and 25–32 DAP are much broader.

The results of the computational deconvolution affording ^{13}C isotopolog excess over the natural abundance contribution in the three experiments are shown in Table 1 and Fig. 4(a). Eight isotopologs carrying two or more ^{13}C-labels had ^{13}C enrichments of more than 0.02 mol% in the present experiments. More specifically, the {110000}, {000011}, {011000}, {000110}, {111000}, {000111}, {001111}, and {111111} isotopologs were found as the major specimens in the group of 15 multiply ^{13}C-labeled isotopologs in all samples. All these isotopologs can be explained by known mechanisms of carbohydrate metabolism in plants (see below). Isotopologs that cannot be explained by standard pathways were observed at abundances below 0.02 mol% indicating the validity of the deconvolution procedure.

Table 1
Distribution of isotopologs of glucose from starch in developing maize kernels (11–18, 18–25, and 25–32 DAP) grown with {111111} glucose

Glucose isotopolog	^{13}C excess (mol%)					
	DAP 11–18		DAP 18–25		DAP 25–32	
	Exp.	Sim.	Exp.	Sim.	Exp.	Sim.
{100000}	0.08	0.07	0.03	0.03	0.09	0.09
{010000}	0.05	0.05	0.00	0.00	0.06	0.05
{001000}	0.34	0.21	0.18	0.08	0.18	0.13
{000100}	0.17	0.14	0.11	0.09	0.12	0.1
{000010}	0.00	0.00	0.01	0.01	0.02	0.02
{000001}	0.00	0.02	0.02	0.02	0.04	0.03
{110000}	0.37	0.31	0.23	0.19	0.14	0.12
{000011}	0.22	0.25	0.12	0.14	0.11	0.14
{011000}	0.02	0.02	0.05	0.04	0.03	0.03
{000110}	0.04	0.03	0.02	0.02	0.02	0.02
{111000}	0.78	0.79	0.59	0.62	0.41	0.43
{000111}	0.93	0.99	0.70	0.78	0.48	0.52
{001111}	0.08	0.08	0.01	0.01	0.02	0.02
{111111}	0.25	0.25	0.18	0.18	0.17	0.17
Deviation[a]		10.8%		13.3%		10.6%

Experimentally obtained values for ^{13}C excess in mol% (Exp.) are compared with the simulated ^{13}C excess (Sim.) using the transfer rules in Supplemental Table 4.

[a] The deviation d between the experimentally determined isotopolog excess e_i and the simulated isotopolog excess s_i is defined as $d = \frac{\sum |e_i - s_i|}{\sum e_i}$.

The {111111} isotopolog representing the fraction of labeled glucose molecules that were embedded into kernel starch without prior metabolic processing was detected at low abundance (0.17–0.25 mol%, cf. Table 1) in all starch samples. We conclude that most glucose molecules undergo metabolic processing before being converted into starch. This is in line with our earlier observations (Glawischnig et al., 2002). Notably, the abundances of multiply ^{13}C-labeled isotopologs, as well as the abundances of

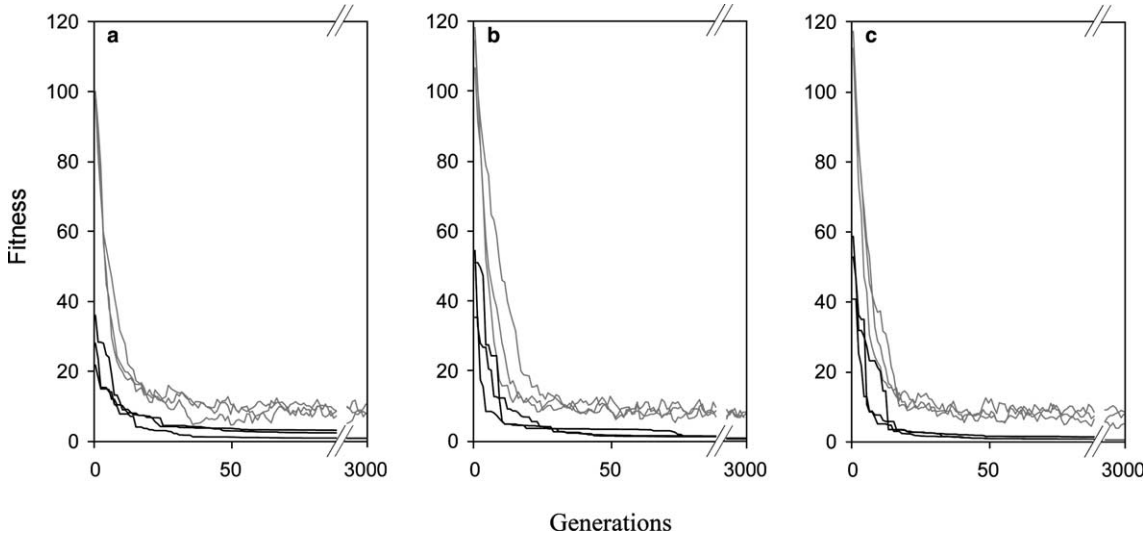

Fig. 3. Evolution processes for computational deconvolution of isotopolog abundances using a genetic algorithm. All iterations show a continuous decline of the deviation between glucose X groups and isotopologs for 3 representative populations. All processes converge between 1750 and 3000 generations. Black lines indicate the course of optimization of the best individuum within a population, while gray lines show the average fitness of the population. (a) Deconvolution for sample 11–18 DAP. (b) Deconvolution for sample 18–25 DAP. (c) Deconvolution for sample 25–32 DAP.

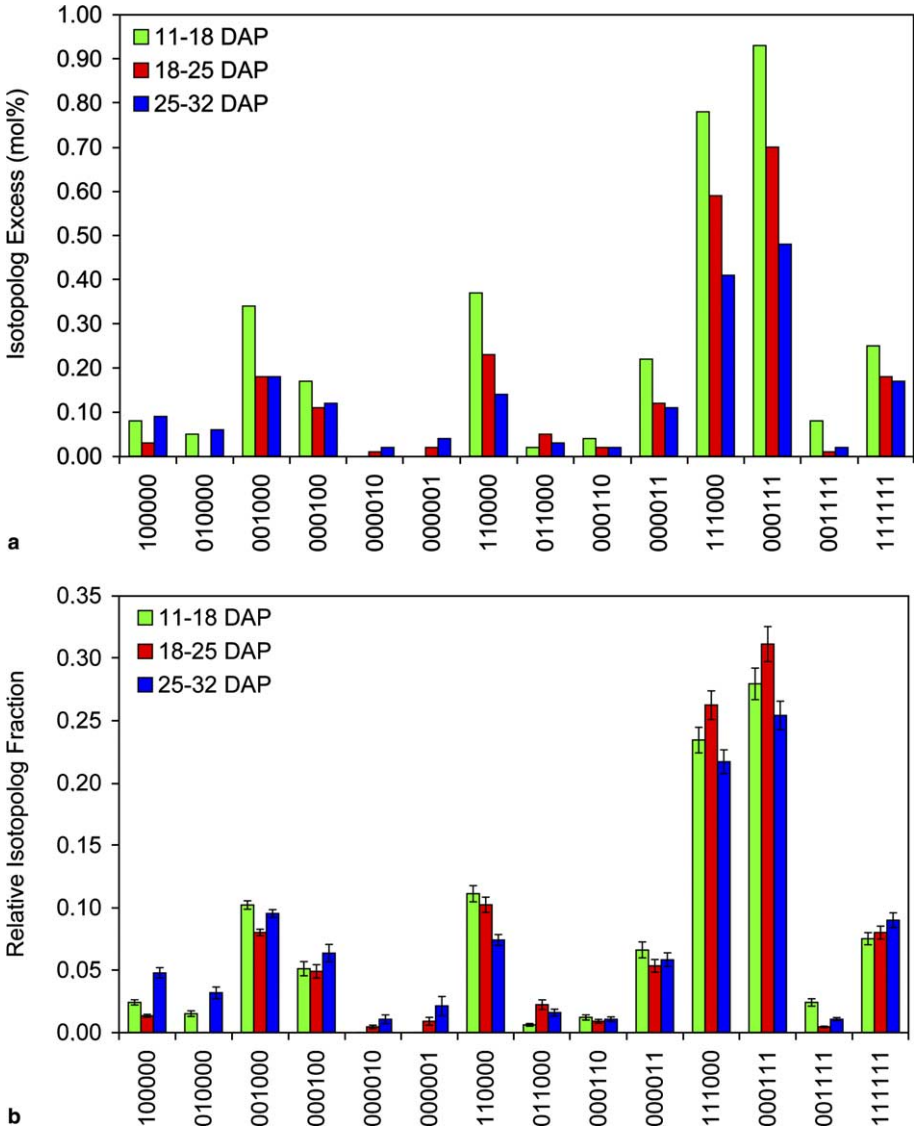

Fig. 4. Glucose isotopolog excess over natural abundance (a) in starch hydrolysates obtained from developing maize kernels after labeling with [U–$^{13}C_6$]glucose (11–18 DAP, 18-22 DAP, and 25–32 DAP). The excess of a specific isotopolog was normalized to the total excess of all isotopologs in a given labeling experiment (b). The SDs for the quantification of individual isotopologs were taken from reproducibility experiments illustrated in Supplementary Information 1.

single- labeled isotopologs showed significant changes during the intervals under study (Fig. 4(a)).

In order to enable a quantitative comparison between the labeling data from the three time intervals, we normalized the isotopolog excess of each isotopolog to the sum of the isotopolog excess (cf. Table 1) in a given experiment (Fig. 4(b)). This normalization is necessary since the amounts of preformed natural abundance starch were different in the three labeling periods.

The {000111} and {111000} isotopologs, which have the highest normalized abundance among the 21 isotopologs in each labeling interval, can be explained predominantly by glycolytic cleavage of {111111} glucose into {111} triose phosphates and subsequent regeneration of hexose phosphate ("emp" in Figs. 5 and 6). Moreover, the PPP can also produce {111} triose phosphate from {11111} xylulose 5-phosphate through the transketolase forward reaction, or from {111111} fructose 6-phosphate through the transaldolase reverse reaction. Regeneration of glucose from {111} triose phosphates via the aldolase/triose phosphate isomerase triangle (Kruger et al., 2003) would typically introduce a partner molecule derived from a non-labeled glucose molecule (i.e., from {000000}). Assuming that the triose phosphates are in equilibrium, these reactions would be expected to afford equal amounts of the {000111} and {111000} glucose isotopologs. However, a sizeable excess of the {000111} over the {111000} isotopolog was observed in all experiments (Fig. 4(b)). This excess can be explained by the transaldolase forward reaction of the non-oxidative PPP that lead to {000111} fructose 6-phosphate, but not to the {111000} isotopolog. Specifically, {000111} fructose 6-phosphate can be formed from {111} glyceraldehyde

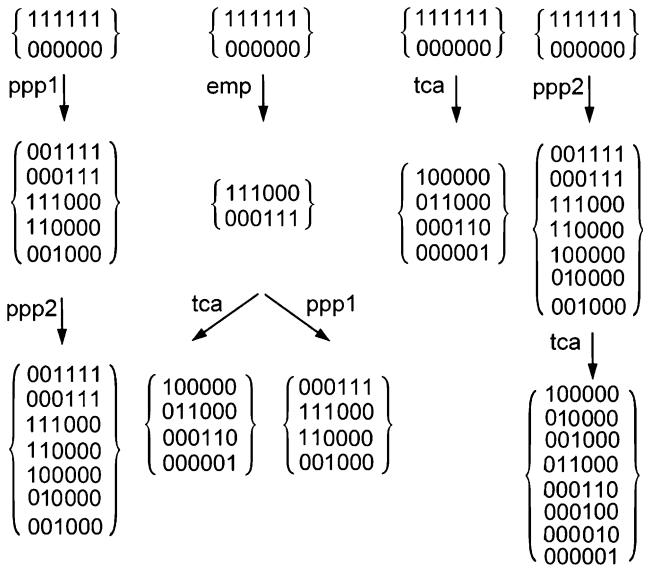

Fig. 5. Metabolic grammar used in the simulation of isotopolog compositions in starch glucose in labeling experiments with [U–$^{13}C_6$]glucose. Glycolytic cycling involving glycolysis (“emp”), the full oxidative PPP (“ppp1”), the non-oxidative PPP (“ppp2”), and the regeneration of glucose via oxaloacetate (“tca”) lead to specific sets of isotopologs (see also Supplemental Table 4). For details of the X group notation, see text.

3-phosphate and unlabeled {0000000} sedoheptulose 7-phosphate in the transaldolase forward reaction. The formation of the orthogonal {111000} fructose 6-phosphate in this reaction would imply {000} glyceraldehyde phosphate and {111XXXX} sedoheptulose 7-phosphate as substrates. However, the formation of {111XXXX} sedoheptulose 7-phosphate requires {11XXX} xylulose 5-phosphate and {1XXXX} ribose 5-phosphate as substrates in the transketolase reaction of the PPP. Since the proffered {111111} glucose is highly diluted with unlabeled glucose in the culture medium, anabolic processes using two ^{13}C-labeled fragments are negligible. The ratio of the {000111} over the {111000} isotopolog abundance is therefore related to the forward velocity of transaldolase. This ratio was calculated as 1.19, 1.19, and 1.17 in the 11–18, 18–25, and 25–32 DAP samples, respectively, indicating that the forward velocity of transaldolase did not change significantly during kernel development. The full PPP according to accepted biochemistry converts three molecules of glucose 6-phosphate into two molecules of fructose 6-phosphate and one molecule of triose phosphate with the release of three molecules of carbon dioxide. Glucose 6-phosphate can subsequently be regenerated from these products by glycolytic reactions. This process was previously identified as one of the elementary flux modes of the glycolysis/PPP-network (Schuster et al., 2000), and is implemented as “ppp1” in the simulation of carbohydrate metabolism here (Figs. 5 and 6). The reaction sequence of “ppp1” generates the hexose phosphate isotopologs {110000}, {001111}, {001000}, and {000111}. It also yields {111} triose phosphates which give rise to equal amounts of {000111} and {111000} through glucogenesis (cf. “ppp1” in Supplemental Table 4). Except for {001111}, which is subject to further scrambling of label, these isotopologs are present at high abundances in all three experiments.

All the reactions of the non-oxidative PPP are assumed to be reversible, allowing this part to work in both directions. This enables the reversible cycling between five hexoses and six pentoses. Both directions of this pathway were identified as individual elementary flux modes (Schuster et al., 2000). These flux modes were combined into the circular “ppp2” process that is used to represent the non-oxidative PPP in this study (Figs. 5 and 6). The conversion of {111111} hexose phosphates into pentose phosphates yields the pentose isotopologs {00111}, {10000}, {11000}, and {01111}. When these pentoses are converted back into hexoses, the glucose isotopologs {010000} and {100000} are generated in addition to the set of isotopologs that is also generated in the “ppp1” process. The “ppp1” and “ppp2” processes also differ with respect to the stoichiometry of isotopolog transformations. For example, the isotopolog ratio of {000111} over {111000} generated from {111111} hexoses in “ppp1” and “ppp2” is 3.0 and 4.3, respectively (cf. Supplemental Table 4). The cleavage and reassembly of carbon backbones through the PPP is restricted to the carbon–carbon bonds between C-1 and C-4 of the glucose molecule. Therefore, the isotopologs {100000}, {010000}, and {001000}, but not {000100}, {000010}, and {000001}, can be generated directly in this process (“ppp1” and “ppp2”).

The formation of the isotopolog pairs {011000}, {100000}, {000110}, and {000001} isotopologs can be explained by the action of the citrate cycle and gluconeogenesis with [1,2-$^{13}C_2$]- or [3,4-$^{13}C_2$]oxaloacetate as precursors, respectively (Eisenreich et al., 2004) (“tca” in Figs. 5 and 6). Notably, the {011000} and {000110} isotopologs could not be detected in our earlier study (Glawischnig et al., 2002) due to the limitations of the method that was available at that time.

In order to quantify the fractions of each metabolic process in the overall glucose cycling prior to starch formation, specific isotopolog transformation rules (Supplemental Table 4) derived from these processes were implemented in the 4F algorithm (Ettenhuber and Eisenreich, 2005). Each process involves the uptake of external glucose followed by a circular pathway that consumes and regenerates hexose phosphate. Finally, regenerated hexose phosphate is converted into starch. The individual circular pathways (shown in Fig. 6) were modeled by rules instead of functions (for additional information of computer models of complex systems, see Yourdon, 1989 and Powel-Douglass, 2004). Functional-based flux simulations (Schmidt et al., 1997, 1998; Follstadt and Stephanopoulos, 1998; Fiaux et al., 1999; Wiechert et al., 1997) are based on numerical calculations estimating the probability of forward and reverse metabolite fluxes through given biochemical reactions (Gillespie, 1977). In contrast to these approaches, the metabolic rules given in Supplemental Table 4 are aimed to estimate flux contributions of metabolic processes typically

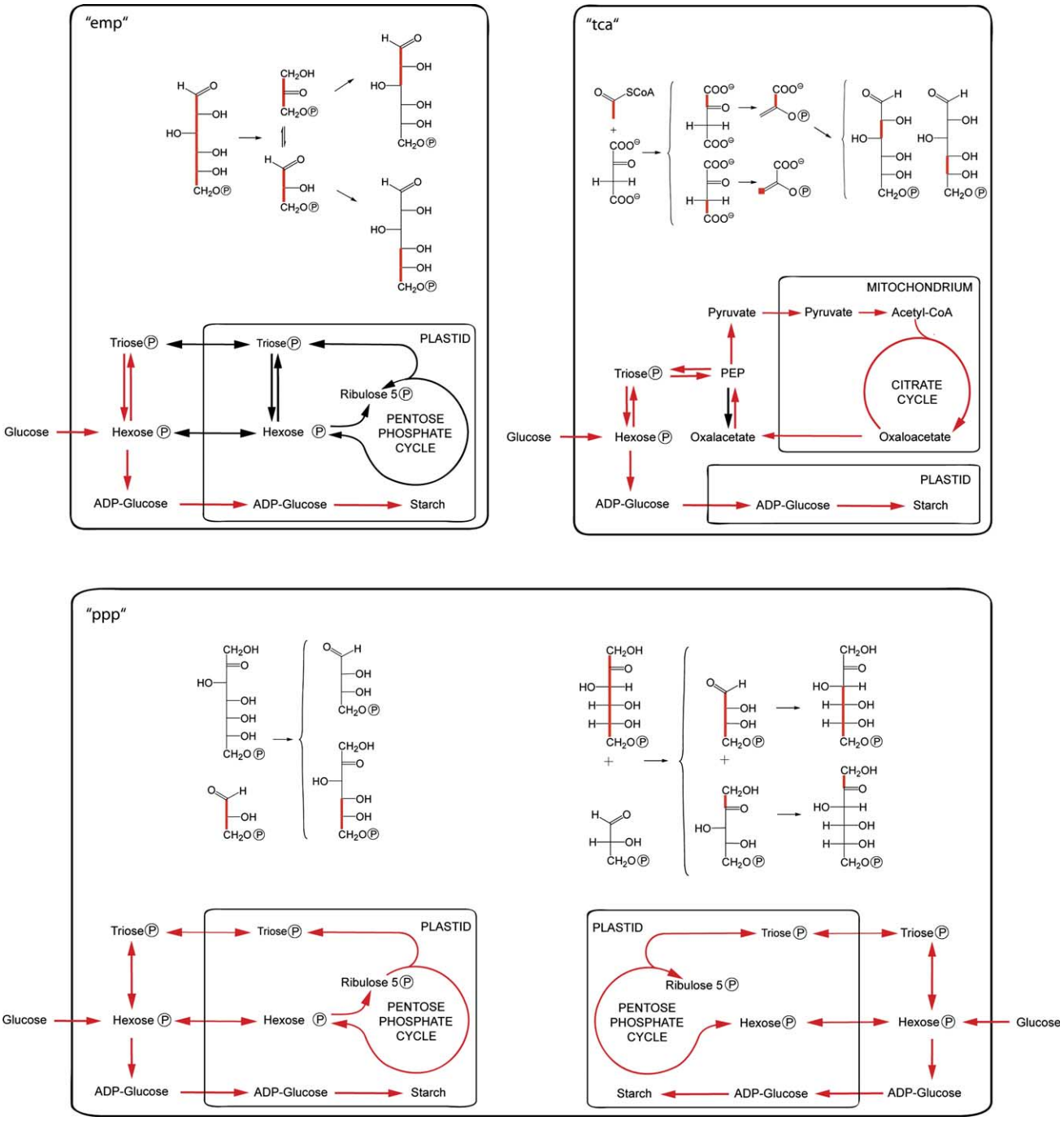

Fig. 6. Metabolic processes contributing to the cycling of hexose-phosphates prior to starch biosynthesis in developing maize kernels. The carbohydrate metabolism was formally divided into five pathways that lead from externally supplied glucose to starch-bound glucose, respectively. These pathways are indicated by red arrows in the metabolic network (see text for details). The figure shows the action of glycolysis and glucogenesis (''emp''), the citric acid cycle and gluconeogenesis (''tca''), and the pentose phosphate pathway (''ppp'') which is represented by two separate modes of action, the full oxidative PPP (left panel) and the non-oxidative PPP (right panel). The isotopologs generated by the transaldolase reaction and the transketolase reaction are shown. For the generation of the additional isotopologs encoded by the metabolic transfer rules ''ppp1'' and ''ppp2'', see text. The direct transfer of glucose into starch without prior remodeling (''dtr'') is not shown. The reactions leading to specific isotopolog patterns (red bars indicate adjacent ^{13}C atoms) are shown. Rules for isotopolog transformations were derived on the basis of each pathway and used to infer its relative contribution to glucose cycling (cf. Supplemental Table 4). (For interpretation of the references in color in this figure legend, the reader is referred to the web version of this article.)

involving large sets of reactions in the metabolic network. The rules implemented in the 4F software are based on the topology of $^{13}C^{13}C$ coupling patterns as a result of specific reactions in a given cycle. The simulated isotopolog excess is shown in Table 1 and deviates by 10–13% from the spectroscopically obtained isotopolog excess in the

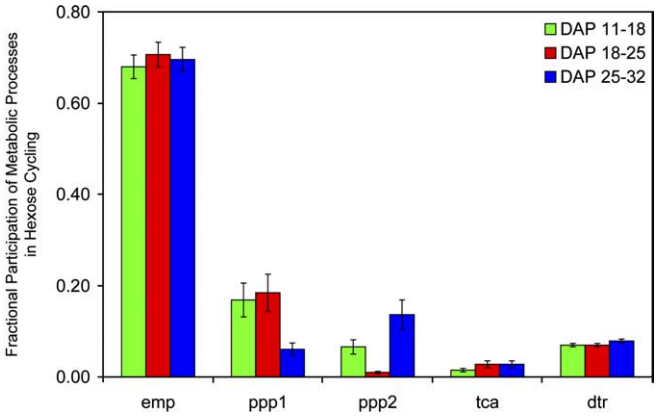

Fig. 7. Results of in silico simulations of maize kernel carbohydrate metabolism. Contributions of individual pathways to the metabolic processing of glucose in the intervals 11–18, 18–25, and 25–32 DAP are given as relative fractions of all applied isotopolog conversions in the simulation.

three experiments (see Table 1 for details). It can be concluded that the metabolic processes implemented in the 4F software (cf. Fig. 6) are sufficient to describe the major contributions to glucose metabolism in maize kernels.

The results of the simulations are summarized in Fig. 7 and Supplemental Table 5. Cycling between triose phosphates and hexose phosphates is revealed as the dominant process of carbohydrate metabolism during starch synthesis in maize (“emp”). Interestingly, the simulation shows a major switch from an oxidative to a non-oxidative operational mode of the PPP towards the end of kernel development. The first and second labeling periods (11–18 and 18–25 DAP) are characterized by a higher activity of the full oxidative PPP (“ppp1”) as compared to the late period. Conversely, in the third period (25–32 DAP) the activity of “ppp2” was highest. The middle phase was characterized by the lowest contribution of “ppp2”. The interplay of glucose 6-phosphate with the citric acid cycle through regeneration of phosphoenolpyruvate from oxaloacetate was slightly higher in the middle and late periods than in the early period of the experiment (“tca”).

3. Discussion

In a previous study, we showed by isotopolog perturbation/relaxation analysis that most glucose molecules entering a maize kernel are subjected to metabolic remodeling prior to the incorporation into starch (Glawischnig et al., 2002). In the earlier study, developing maize kernels were ^{13}C-labeled for three weeks. The observed isotopolog pattern therefore represented an average of carbohydrate metabolism during the majority of the starch deposition phase. An improved NMR analysis and greater sensitivity of isotopolog detection allowed us to reduce the length of the ^{13}C-labeling pulse to 7 days. This enabled three separate labeling experiments for successive intervals of kernel development with the aim of detecting possible changes of metabolic patterns. The abundances of 21 isotopologs in glucose derived from kernel starch were determined as described (Eisenreich et al., 2004; Ettenhuber et al., 2005). It is justified to consider only this set of 21 isotopologs out of the possible 64 isotopologs of glucose because the other isotopologs can be assumed to be generated in negligible amounts in the chosen experimental setup, i.e., with unlabeled glucose in high excess over the ^{13}C-labeled tracer (for a detailed discussion, see also Eisenreich et al., 2004; Glawischnig et al., 2002).

The computational deconvolution of isotopologs used 45 X groups of glucose, from which 224 positive constraints and 721 negative constraints were derived. It should be noted in this context that the number of X groups in a given experiment depends to a significant degree on experimental details such as spectral resolution and isotopolog abundance; broad lines and low isotopolog abundances present unfavorable conditions. The lower number of X groups available for the sample from the late period of starch deposition was mainly due to the relatively low abundance of multiply labeled isotopologs in that sample. However, even in that experiment, the initial data set was overdetermined because the number of X group constraints exceeds the number of unknown isotopolog concentrations. Moreover, we showed that the omission of certain X groups from the initial data sets (i.e., the use of initial data sets with a lower degree of overdetermination) did not significantly change the results. By using our method, 15 isotopologs containing two or more ^{13}C atoms can be quantified individually. However, among this set of 15 isotopologs, only 8 were formed in significant amounts.

The quantification of metabolic processes that shaped the isotopolog patterns revealed glycolysis/glucogenesis (“emp”) and the PPP as the dominant fluxes for all studied intervals in the developing maize kernels (Fig. 7). These two processes were also dominant in maize root tips (Dieuaide-Noubhani et al., 1995; Edwards et al., 1998), *B. napus* (Schwender et al., 2003), soybean embryos (Sriram et al., 2004), and tobacco plants (Ettenhuber et al., 2005), respectively. Therefore, it is possible that the organization of core fluxes in the central carbohydrate metabolism is conserved across distantly related plant species. However, we also observed significant changes in the metabolic pattern during kernel development. Especially, the contributions of the different modes of PPP (“ppp1” and “ppp2”) were found to be modified in the different experimental periods with a significantly lower contribution of the non-oxidative PPP (“ppp2”) during the middle phase. Such a flexibility of core fluxes was not observed in tomato cells in suspension culture (Rontein et al., 2002). Changes of flux patterns in maize kernels on one hand and “metabolic stability” of tomato suspension cells on the other hand may reflect the fact that maize kernel tissues are subject to developmental changes while cells in suspension culture are not.

A possible explanation for the changes of metabolic fluxes in maize kernels, although entirely speculative, is based on the observation that the fractional allocations of carbon to the major storage compounds, i.e., starch,

protein, and lipids, change during development. More specifically, after a lag phase that follows pollination, starch deposition generally occurs in a linear fashion (Singletary et al., 1997). Likewise, the rate of lipid synthesis is nearly constant (Ingle et al., 1965). However, the rates of protein accumulation are high at the beginning and at the end of the linear filling phase, while there is only little increase of total protein in the middle phase of kernel development (Ingle et al., 1965). Since many amino acids are derived from intermediates of the non-oxidative PPP (''ppp2''), the increased metabolic activity involving this process may serve to accommodate the increased demand for amino acid precursors in the early and late phase of maize kernel development. In order to further substantiate this hypothesis, the analysis of metabolic fluxes is necessary in maize lines that are selected for high protein or high oil content (Moose et al., 2004) and in mutants affecting starch accumulation (Boyer and Hannah, 2001).

4. Experimental

4.1. Plant material and tissue culture

Maize plants of the inbred line W22 were grown in the field in Gainesville, FL. Ears were harvested 8–10 days after pollination (DAP) and processed as described (Glawischnig et al., 2002) with the following modifications. Protruding silks were cut off and 2 layers of outer husks were removed. The ear was sprayed with ethanol and flamed. After removing the inner husks and silks, the ear was dissected into two-row pieces with a total of 4–10 attached kernels. The kernel blocks were placed in 25×100 mm Petri dishes containing 50 ml of culture medium (cf. Fig. 1(a)). The culture medium contained 4.3 g of Murashige-Skoog salts, 1.0 g of casein hydrolysate, 20 mg of gentamycine, 3.5 g of agar, 1.0 mg of 2,4-dichlorophenoxyacetic acid and 80 g of glucose per liter. The pH was adjusted to 5.8 prior to autoclaving.

Kernel blocks were initially cultured on unlabeled medium and incubated at 28 °C in the dark. At 11, 18 or 25 days after pollination, individual kernel blocks were transferred to fresh Petri dishes containing 2.7 g of [U–$^{13}C_6$]glucose and 77.3 g of unlabeled glucose per liter of medium. They were harvested after incubation for 7 days.

For the determination of kernel dry weights, kernels were cultured as described above except that the W22 maize donor plants were grown in the greenhouse. Kernels were harvested between 9 and 38 DAP and lyophilized. Dry weights were determined based on samples of at least 10 kernels.

4.2. Isolation of glucose from starch

Frozen kernels were ground in liquid nitrogen and the powder (200 mg) was extracted three times with *n*-hexane. To remove soluble sugars, the residue was extracted three times with 80% (v/v) ethanol for 15 min at 60 °C. The residue was treated with 2 ml of 0.5 M NaOH for 1 h at 65 °C in order to gelatinize starch. The mixture was diluted with 12 ml of water, adjusted to pH 4.5 with 1 M acetic acid, and centrifuged (45 min, 4800 rpm). Amyloglucosidase (120 U, lyophilized powder from Sigma–Aldrich) was added to the supernatant. The mixture was incubated at 55 °C for 3 h and was then centrifuged (45 min, 4,800 rpm). The supernatant was concentrated under reduced pressure. The residue was dissolved in 2 ml of 0.2 M ammonium acetate, pH 8.8. The solution was adjusted to pH 9.0 with 1 M NaOH. Glucose was isolated by affinity chromatography using a 2-ml Affigel 601 column (Bio-Rad, Hercules, CA) . The column was equilibrated and washed with 0.2 M ammonium acetate, pH 8.8, and developed with 0.2 M ammonium acetate, pH 6.0. Fractions of 1 ml were collected and assayed for glucose by thin layer chromatography on Silica gel 60 (Merck) plates which were developed with chloroform/acetic acid/water 6:7:1 (v/v). Glucose was detected by spraying with ethanolic solution of 5% (m/V) trichloracetic acid, 2.5% (m/V) phtalic acid and 0.6% (m/V) 4-aminohippuric acid and heating to 120 °C for 10 min. Glucose-containing fractions were combined and dried. The residue was dissolved in water, and glucose was further purified on a Rezex RPM-Monosaccharide HPLC column (Phenomenex, 300×7.8 mm) that was developed with water (0.4 ml min^{-1}; 80 °C). Glucose had a retention time of 22.5 min and was dried under reduced pressure.

4.3. NMR spectroscopy and data analysis

Glucose was dissolved in 0.5 ml of D_2O. ^1H and ^{13}C NMR spectra were recorded at 500.13 and 125.76 MHz, respectively, using a Bruker DRX500 spectrometer, at 27 °C. The experimental setup, signal assignments, coupling constants and isotope shifts of α- and β-glucose have been reported earlier (Eisenreich et al., 2004).

The analysis of ^{13}C abundance and isotopolog composition was performed as described (Eisenreich et al., 2004). Briefly, in the ^1H-decoupled ^{13}C NMR spectrum, each line was integrated separately. The relative fractions of each respective satellite pair (corresponding to the relative abundance of certain X groups) in the total signal integral of a given carbon atom were calculated (Supplemental Tables 1 and 2). These values were then referenced to the global ^{13}C abundance of glucose obtained from isotope ratio mass spectrometry (mol% in Supplemental Table 3).

The ^{13}C abundances of individual glucose isotopologs (cf. Table 1) were obtained by computational deconvolution of X group abundance using a genetic algorithm (for details, see Ettenhuber and Eisenreich, 2005; Eisenreich et al., 2004; parameters: number of populations, 12; population size, 50; generation gap, 0.95; mutation rate, 0.01; cross-over rate, 0.9). Multiple-labeled isotopologs within the noise-level were constrained as illegal terrain. The ^{13}C enrichments (excess) were obtained from the ^{13}C abundances by subtracting the natural abundance contributions

for each isotopolog. Normalized enrichments v_i were then calculated from the ^{13}C enrichments e_i of each isotopolog by applying $v_i = \frac{e_i}{\sum_{k=0}^{J} e_i}$.

The reconstruction of metabolic pathways was performed using the 4F software described in Ettenhuber et al. (2005) and Ettenhuber and Eisenreich (2005). The rule set of the simulation software was modified according to Supplemental Table 4.

Error analysis for the isotopolog deconvolution and the metabolic simulation was based on the SDs of individual isotopologs obtained from a triplicate with W22 kernels (for details, see Supplemental Information 1).

4.4. Isotope ratio mass spectrometry

After NMR analysis the glucose samples were lyophilized, and global ^{13}C enrichments were determined by isotope ratio mass spectrometry (Isolab GmbH, Germany; Pillonel et al., 2004).

Acknowledgments

This work was supported by grants from the Deutsche Forschungsgemeinschaft, the Fonds der Chemischen Industrie, the Hans Fischer Gesellschaft and the National Science Foundation (L.C.H.-IBN-9316887, IBN-960416, IBN-9982626 and MCB-9420422), the USDA Competitive Grants Program (L.C.H. 94-37300-453, 9500836, 95-37301-2080, 9701964, 97-36306-4461, 98-01006 and 2000-01488), and the Florida Agricultural Experiment Station. We thank Fritz Wendling and Christine Schwarz for expert technical assistance.

Appendix A. Supplementary data

Supplementary data associated with this article can be found, in the online version, at doi:10.1016/j.phytochem.2005.09.017.

References

Arabidopsis Genome Initiative, 2001. Analysis of the genome sequence of the flowering plant *Arabidopsis thaliana*. Nature 408, 796–815.

Ball, S.G., Morell, M.K., 2003. From bacterial glycogen to starch, understanding the biogenesis of the plant starch granule. Annu. Rev. Plant Biol. 54, 207–233.

Boyer, C.D., Hannah, L.C., 2001. Kernel mutants of corn. In: Hallauer, A.R. (Ed.), Specialty Corns. CRC Press, Boca Raton, FL, pp. 1–31.

Dieuaide-Noubhani, M., Raffard, G., Canioni, P., Pradet, A., Raymond, P., 1995. Quantification of compartmented metabolic flux in maize root tips using isotope distribution from ^{13}C- or ^{14}C-labeled glucose. J. Biol. Chem. 270, 13147–13159.

Duvick, D.N., 2001. Biotechnology in the 1930s, the development of hybrid maize. Nat. Rev. Genet. 2, 69–74.

Edwards, S., Nhuyen, B.T., Do, B., Roberts, J.K.M., 1998. Contribution of malic enzyme, pyruvate kinase, phosphoenolpyruvate carboxylase, and the Krebs cycle to respiration and biosynthesis and to intracellular pH regulation during hypoxia in maize root tips observed by nuclear magnetic resonance imaging and gas chromatography–mass spectrometry. Plant Physiol. 116, 1073–1081.

Eisenreich, W., Ettenhuber, C., Laupitz, R., Theus, C., Bacher, A., 2004. Isotopolog perturbation techniques for metabolic networks, metabolic recycling of nutritional glucose in *Drosophila melanogaster*. Proc. Natl. Acad. Sci. USA 101, 6764–6769.

Ettenhuber, C., Eisenreich, W., 2005. 4F Service 1.1, Type 2 Network. Available from: <http://xsystem.org.chemie.tu-muenchen.de>.

Ettenhuber, C., Radykewicz, T., Kofer, W., Koop, H.U., Bacher, A., Eisenreich, W., 2005. Metabolic flux analysis in complex isotopologous space. Recycling of glucose in tobacco plants. Phytochemistry 66, 323–335.

Fiaux, J., Andersson, C.J.Y., Holmberg, N., Bülow, L., Kallio, P.T., Szyperski, T., Bailey, J.E., Wüthrich, K., 1999. ^{13}C NMR flux ratio analysis of *Escherichia coli* central carbon metabolism in microaerobic bioprocesses. J. Am. Chem. Soc. 121, 1407–1408.

Follstadt, B.D., Stephanopoulos, G., 1998. Effect of reversible reactions on isotope label redistribution – analysis of the pentose phosphate pathway. Eur. J. Biochem. 202, 360–371.

Gillespie, D.T., 1977. Exact stochastic simulation of coupled chemical reactions. J. Phys. Chem. 81, 2340–2361.

Glawischnig, E., Gierl, A., Tomas, A., Bacher, A., Eisenreich, W., 2001. Retrobiosynthetic NMR analysis of amino acid biosynthesis and intermediary metabolism, metabolic flux in developing maize kernels. Plant Physiol. 125, 1178–1186.

Glawischnig, E., Gierl, A., Tomas, A., Bacher, A., Eisenreich, W., 2002. Starch biosynthesis and intermediary metabolism in maize kernels. Quantitative analysis of metabolite flux by nuclear magnetic resonance. Plant Physiol. 130, 1717–1727.

Goff, S.A., Ricke, D., Lan, T.-H., Presting, G., Wang, R., Dunn, M., Glazebrook, J., Sessions, A., Oeller, P., Varma, H., Hadley, D., Hutchison, D., Martin, C., Katagiri, F., Lang, B.M., Moughamer, T., Xia, Y., Budworth, P., Zong, J., Miguel, T., Paszkowski, U., Zhang, S., Colbert, M., Sun, W.-L., Chen, L., Cooper, B., Park, S., Wood, T.C., Mao, L., Quail, P., Wing, R., Dean, R., Yu, Y., Zharkikh, A., Shen, R., Sahasrabudhe, S., Thomas, A., Cannings, R., Gutin, A., Pruss, D., Reid, J., Tavtigian, S., Mitchell, J., Eldredge, G., Scholl, T., Miller, R.M., Bhatnagar, S., Adey, N., Rubano, T., Tusneem, N., Robinson, R., Feldhaus, J., Macalma, T., Oliphant, A., Briggs, S., 2002. A draft sequence of the rice genome (*Oryza sativa* L. ssp. *japonica*). Science 296, 92–100.

Ingle, J., Bietz, D., Hageman, R.H., 1965. Metabolic changes associated with the germination of corn. Plant Physiol. 40, 832–835.

James, M.G., Denyer, K., Myers, A.M., 2003. Starch synthesis in the cereal endosperm. Curr. Opin. Plant Biol. 6, 215–222.

Kruger, N.J., Ratcliffe, R.G., Roscher, A., 2003. Quantitative approaches for analysing fluxes through plant metabolic networks using NMR and stable isotope labelling. Phytochem. Rev. 2, 17–30.

Moose, S.P., Dudley, J.W., Rocheford, T.R., 2004. Maize selection passes the century mark, a unique resource for 21st century genomics. Trends Plant Sci. 9, 358–364.

Pillonel, L., Bütikofer, U., Rossmann, A., Tabacchi, R., Bosset, J.O., 2004. Analytical methods for the detection of adulteration and mislabelling of Raclette Suisse® and Fontina PDO cheese. Mitt. Lebensm. Hyg. 95, 489–502.

Powel-Douglass, B., 2004. Real Time UML. Addison-Wesley, New York.

Rontein, D., Dieuaide-Noubhani, M., Dufourc, E.J., Raymond, P., Rolin, D., 2002. The metabolic architecture of plant cells. Stability of central metabolism and flexibility of anabolic pathways during the growth cycle of tomato cells. J. Biol. Chem. 277, 43948–43960.

Schmidt, K., Carlsen, M., Nielsen, J., Villadsen, J., 1997. Modeling isotopomer distributions in biochemical networks using isotopomer mapping matrices. Biotechnol. Bioeng. 55, 831–840.

Schmidt, K., Marx, A., deGraaf, A.A., Wiechert, W., Sahm, H., Nielsen, J., Villadsen, J., 1998. ^{13}C tracer experiments and metabolite balancing for metabolic flux analysis, comparing two approaches. Biotechnol. Bioeng. 58, 254–257.

Schultz, J.A., Juvik, J.A., 2004. Current models for starch synthesis and the sugary enhancer1 (se1) mutation in *Zea mays*. Plant Physiol. Biochem. 42, 457–464.

Schuster, S., Fell, D.A., Dandekar, T., 2000. A general definition of metabolic pathways useful for systematic organization and analysis of complex metabolic networks. Nat. Biotechnol. 18, 326–332.

Schwender, J., Ohlrogge, J.B., Shachar-Hill, Y., 2003. A flux model of glycolysis and the oxidative pentosephosphate pathway in developing *Brassica napus* embryos. J. Biol. Chem. 278, 29442–29453.

Schwender, J., Ohlrogge, J.B., Shachar-Hill, Y., 2004. Understanding flux in plant metabolic networks. Curr. Opin. Plant Biol. 7, 309–317.

Singletary, G.W., Banisadr, R., Keeling, P.L., 1997. Influence of gene dosage on carbohydrate synthesis and enzymatic activities in endosperm of starch-deficient mutants of maize. Plant Physiol. 113, 293–304.

Sriram, G., Fulton, D.B., Iyer, V.V., Peterson, J.M., Zhou, R., Westgate, M.E., Spalding, M.H., Shanks, J.V., 2004. Quantification of compartmented metabolic fluxes in developing soybean embryos by employing biosynthetically directed fractional ^{13}C labeling, two-dimensional [^{13}C, ^{1}H] nuclear magnetic resonance, and comprehensive isotopomer balancing. Plant Physiol. 136, 3043–3057.

Wiechert, W., Siefke, C., de Graaf, A.A., Marx, A., 1997. Bidirectional reaction steps in metabolic networks Part II: flux estimation and statistical analysis. Biotechnol. Bioeng. 55, 118–135.

Yamada, K., Lim, J., Dale, J.M., Chen, H., Shinn, P., Palm, C.J., Southwick, A.M., Wu, H.C., Kim, C., Nguyen, M., Pham, P., Cheuk, R., Karlin-Newmann, G., Liu, S.X., Lam, B., Sakano, H., Wu, T., Yu, G., Miranda, M., Quach, H.L., Tripp, M., Chang, C.H., Lee, J.M., Toriumi, M., Chan, M.M.H., Tang, C.C., Onodera, C.S., Deng, J.M., Akiyama, K., Ansari, Y., Arakawa, T., Banh, J., Banno, F., Bowser, L., Brooks, S., Carninci, P., Chao, Q., Choy, N., Enju, A., Goldsmith, A.D., Gurjal, M., Hansen, N.F., Hayashizaki, Y., Johnson-Hopson, C., Hsuan, V.W., Iida, K., Karnes, M., Khan, S., Koesema, E., Ishida, J., Jiang, P.X., Jones, T., Kawai, J., Kamiya, A., Meyers, C., Nakajima, M., Narusaka, M., Seki, M., Sakurai, T., Satou, M., Tamse, R., Vaysberg, M., Wallender, E.K., Wong, C., Yamamura, Y., Yuan, S., Shinozaki, K., Davis, R.W., Theologis, A., Ecker, J.R., 2003. Empirical analysis of transcriptional activity in the *Arabidopsis* genome. Science 302, 842–846.

Yourdon, E., 1989. Modern Structured Systems Analysis. Prentice-Hall, Englewood Cliffs, NJ.